The winners of the 2012 CAP Best Student Oral Presentation Competition at the CAP Annual Congress, 2012 June 11-15, in Calgary, Alberta are listed on page 133. The extended abstracts of those winners of the CAP prizes who submitted them for publication are reproduced below. Ed.

DISSIPATION MECHANISMS IN THERMOMECHANICALLY-DRIVEN SILICON NITRIDE NANOSTRINGS

BY BRADLEY D. HAUER, ABDUL SUHEL, TUSHAR S. BISWAS, KEVIN S.D. BEACH, AND JOHN P. DAVIS

B.D. Hauer <bhauer @ualberta.ca>, A. Suhel, T.S. Biswas, K.S.D. Beach, and J.P. Davis, Department of Physics, University of Alberta, Edmonton, AB, Canada T6G 2E9

A silicon nitride nanostring is a very interesting nanomechanical device that has the geometry of a doubly-clamped beam [1] but behaves like a string due to its high intrinsic tensile stress [2,3]. The resonance frequency of the nth mode of such a device is given by

$$\nu_n = n\nu_1 = \frac{n}{2L}\sqrt{\frac{\sigma}{\rho}} \qquad (1)$$

where ν_1, σ, ρ, and L are the resonance frequency of the first mode, intrinsic stress, density, and length of the nanostring, respectively [4]. It is also worth noting that the resonance frequency of a nanostring depends only on the length of the device, not its width or thickness. This feature is very useful, since we only need to concern ourselves with the fabrication tolerance in one dimension, as opposed to three.

Because of their unique properties, silicon nitride nanostrings have generated a lot of scientific interest, ranging from applications in mass [5] and temperature sensing [6], to more exotic measurements, such as the observation of quantum motion of a mesoscopic resonator [7]. In each of these applications, the mechanical quality factor (Q) of the device is often used as a figure of merit. Q is proportional to the total energy stored in a system divided by the amount of energy dissipated per cycle and, for devices with a high Q, is defined to be

$$Q = 2\pi \times \frac{\text{Energy Stored}}{\text{Energy Dissipated per Cycle}} = \frac{\nu_n}{\Delta\nu} \qquad (2)$$

where $\Delta\nu$ is the full width at half maximum (FWHM) of the resonance peak [2]. We can see from this equation that at a given frequency, the larger the Q of a device, the narrower the resonance peak. This is advantageous because for a constant area under the curve — as is the case for thermo-mechanical motion — a narrower peak means a larger amplitude and a larger single-to-noise ratio (SNR), making the motion of such a device easier to detect. As well, the narrower the resonance peak, the easier it is to resolve the device's resonance frequency, allowing for improved resolution in sensing applications [5,8]. From these effects, it is easy to see that the higher the Q of a nanostring, the better it will perform in each of its applications. It is therefore important to understand the dissipation mechanisms of a nanostring, which will allow us to increase its Q, thus improving its performance.

SUMMARY

The dissipation mechanisms in silicon nitride nanostrings are investigated by observing their thermomechanically driven motion.

The Qs of our silicon nitride nanostrings are very high (~10^5, see Fig. 2), which results from increasing the amount of energy stored in the devices, due to their high internal tension, while maintaining constant dissipation [2,9]. To understand what causes such a high Q in these devices, and to guide our efforts to push it to even higher values, we have developed a model for Q which incorporates the three main dissipation mechanisms in our nanostrings

$$Q_n = \frac{m\omega_n}{\gamma_n} \approx \frac{m}{\tilde{\gamma}^{\text{visc}}\omega_n^{-1} + \tilde{\gamma}^{\text{anchor}} + \tilde{\gamma}^{\text{bulk}}\omega_n} \qquad (3)$$

Here, m is the mass of the nanostring, and Q_n, ω_n, and γ_n denote the Q factor, angular frequency, and damping coefficient for the nth mode of the nanostring [4]. The tilde decorated quantities are damping coefficients that have been stripped of their mode dependence, corresponding to viscous damping, as well as damping at the anchor points and in the bulk of the nanostring. Our experiment operates in a vacuum of ~10^{-6} torr, which is sufficiently low enough to allow us to neglect viscous damping of our resonator $\left(\tilde{\gamma}^{\text{visc}} \approx 0\right)$ [10]. We can then investigate the other two damping mechanisms by observing the thermomechanically actuated motion of our devices.

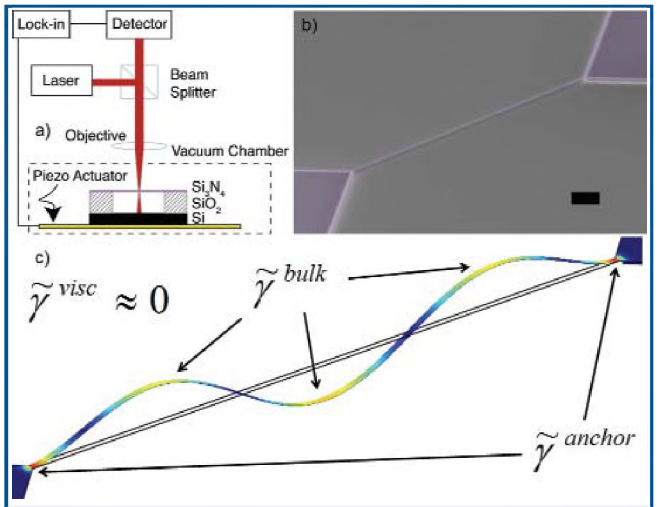

Fig. 1 (a) Schematic of the experimental set-up. (b) Scanning electron microscope image of the 215 µm nanostring. The scale bar is 20 µm. (c) Finite element analysis (FEA) simulation of the 215 µm nanostring. The dissipation locations as decribed in Eq. 3 are labelled.

To detect the motion of our silicon nitride nanostrings, we use the simple optical interferometric setup shown in Fig. 1(a). We exploit the geometry of our system, forming a Fabry-Perot cavity between the silicon nitride nanostring and the silicon base of the chip. As we shine a 632.8 nm HeNe laser through this cavity, the light follows two separate paths, which recombine at the resonator, encoding its motion in the resultant optical interference pattern. This optical signal is then converted to a voltage using a photodetector (PD), which is recorded using a lock-in amplifier (Zurich Instruments HF2LI). The rest of the apparatus consists of an optical access vacuum chamber that houses the sample, as well as a piezoelectric transducer. The piezoelectric allows us to drive the chip at its resonance frequency, increasing the signal and allowing us to find the device's resonant modes.

Once we have found each of these modes, we deactivate the piezoelectric and observe the thermally driven Brownian motion of our nanostrings, using our lock-in amplifier as a spectrum analyzer to record the data. We are then able to calibrate the motion of these resonant modes by utilizing the equipartition theorem, which tells us that each mode of the nanostring contains $k_BT/2$ of thermal energy [11].

The calibration procedure is performed by investigating the measured power spectral density (PSD) of our resonator, which we determine by squaring the recorded voltage data and dividing by the measurement bandwidth. An example of such a spectrum can be seen in the inset of Fig. 2. We then fit to the voltage PSD data the following function[11]

$$S_V(\nu) = S_V^{\mathrm{w}} + \alpha S_z(\nu) \qquad (4)$$

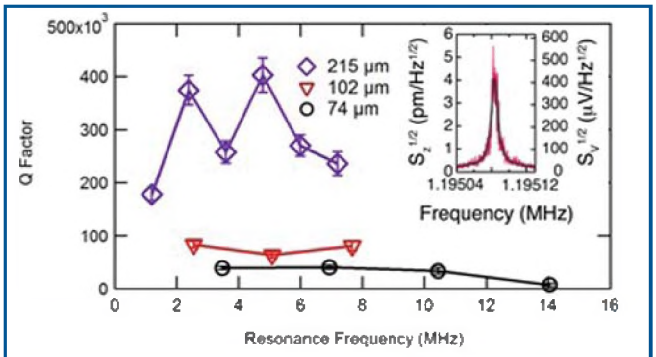

Fig. 2 Plot of mechanical quality factor (Q) vs resonant frequency for three nanostrings. The nanostrings used for this plot have a thickness of 250 nm and widths ranging from 1.0-2.1 µm. Inset – Fitted PSD for the first mode of the 215 µm nanostring, in terms of raw voltage and calibrated displacement.

Here, S_V^w is the white noise of the detector, α is a conversion factor from volts to meters (in units V^2/m^2), and $S_z(\nu)$ is the theoretical PSD for a damped harmonic oscillator as a function of frequency ν. This last term has the form

$$S_z(\nu) = \frac{k_B T \nu_n}{m\pi^3\left[\left(\nu_n^2 - \nu^2\right)^2 + \left(\nu\nu_n / Q\right)^2\right]} \qquad (5)$$

where we have taken $m = \rho lwt$ to be the geometric mass of the nanostring (with l, w, and t being the length, width, and thickness, respectively) using $\rho = 3000$ kg/m^3 as our measured density of the nanostring [4]. From this fit function we can extract the α parameter, allowing us to convert from a PSD in terms of voltage, to one in terms of displacement. We are then able to take the square root of this displacement PSD to determine the peak displacement of our nanostrings in units of $\mathrm{m}/\sqrt{\mathrm{Hz}}$.

By plotting peak displacement vs. resonance frequency, we are able to see a trend emerge, in which there are displacement degeneracies between certain modes of different nanostrings. This can be seen in Fig. 3(a). As the devices we investigated had similar mode shapes and displacements [see Fig. 3(b)], with two anchor points each, the only difference in dissipation mechanisms between these nanostrings is the ratio of dissipation occurring in the bulk to that occurring at the anchor points. Therefore, if the largest nanostring has the highest Q, since it has the most bending points in the bulk of the nanostring, we would expect dissipation at the anchor points to dominate. If the smallest string has the largest Q, however, we would expect dissipation in the bulk of the nanostring to dominate. Looking back at Fig. 2(a), we can see that the largest string does indeed have the highest Q, telling us qualitatively that we would expect dissipation at the anchor points to dominate.

We are also able to quantify the ratio of dissipation in the bulk to dissipation at anchor points by looking at the expected

frequency dependence for the peak displacement Δz of the nanostrings over an arbitrary frequency interval $\Delta\nu$. This is given by

$$\Delta z = \sqrt{S_n\left(\nu_n^{\max}\right)\Delta\nu} \sim \frac{1}{\nu_n^{3/2} + \tau\nu_n^{5/2}} \tag{6}$$

where

$$\tau = \frac{\pi\tilde{\gamma}^{\text{bulk}}}{\tilde{\gamma}^{\text{anchor}}} \tag{7}$$

gives us a quantitative measure of the ratio between these two dissipation mechanisms [4]. From the fit seen in Fig. 3(a), we find that $\tau = (-0.3 \pm 2.5) \times 10^{-7}$s, again confirming that the dissipation mainly occurs at the anchor points in our nanostrings.

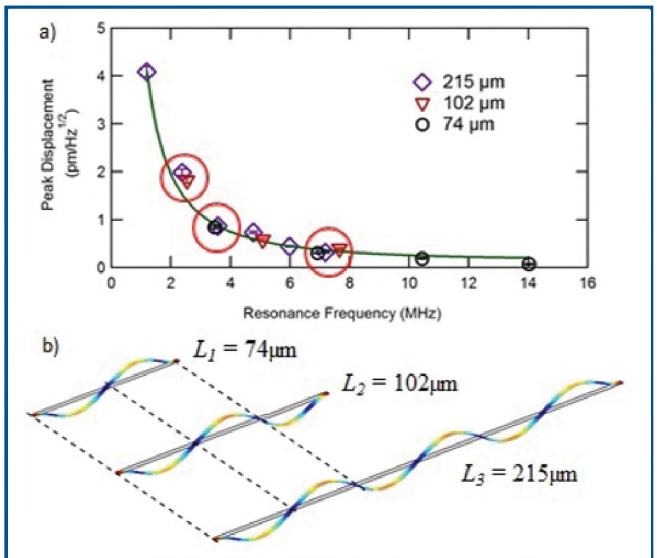

Fig. 3 (a) Peak displacement vs. resonance frequency for the same three nanostrings as in Fig. 2. The solid green line is a fit to Eq. 6. Degeneracies between certain modes of different nanostrings are highlighted with colored circles. (b) FEA simulation showing the mode shapes of all three strings for the highest frequency degeneracy triplet.

In conclusion, by observing a trend in the frequency dependence of the thermally actuated peak displacements of our nanostrings, we were able to pinpoint the location at which the majority of the dissipation occurs in this system. We now wish to focus on understanding what is causing this dissipation. Two leading theories suggest that this damping mechanism is related either to phonons tunneling out of the nanostring at its anchor points [12] or dissipation due to local strain mismatch at the anchor points [13].

Our future work involves using nanostring arrays to isolate and remove phonon tunneling from our nanostrings [14]. It is hoped that by using these structures, we will increase the Q of these devices even further, greatly improving their sensitivity, expanding the horizons for many new applications, as well as improving the ones that already exist.

REFERENCES

1. P. Mohanty, D.A. Harrington, K.L. Ekinci, Y.T. Yang, M.J. Murphy, M.L. Roukes, "Intrinsic dissipation in high-frequency micromechanical resonators", *Phys. Rev. B*, **66**, 085416 (2002).
2. S. Schmid, K.D. Jensen, K.H. Nielsen, A. Boisen, "Damping mechanisms in high-Q micro and nanomechanical string resonators", *Phys. Rev. B*, **84**, 165307 (2011).
3. S.S. Verbridge, J.M. Parpia, R.B. Reichenbach, L.M. Bellan, H.G. Craighead, "High quality factor resonance at room temperature with nanostrings under high tensile stress", *J. Appl. Phys.*, **99**, 124304 (2006).
4. A. Suhel, B.D. Hauer, T.S. Biswas, K.S.D. Beach, J.P. Davis, "Dissipation mechanisms in thermomechanically driven silicon nitride nanostrings", *Appl. Phys. Lett.*, **100**, 173111 (2012).
5. S. Schmid, S. Dohn, A. Boisen, "Real-Time Particle Mass Spectrometry Based on Resonant Micro Strings", *Sensors*, **10**, 8092 (2010).
6. T. Larsen, S. Schmid, L. Grönberg, A.O. Niskanen, J. Hassel, S. Dohn, A. Boisen, "Ultrasensitive string-based temperature sensors", *Appl. Phys. Lett.*, **98**, 121901 (2011).
7. T. Rocheleau, T. Ndukum, C. Macklin, J.B. Hertzberg, A.A. Clerk, K.C. Schwab, "Preparation and detection of a mechanical resonator near the ground state of motion", *Nature*, **463**, 72 (2010).
8. A.K. Naik, M.S. Hanay, W.K. Hiebert, X.L. Feng, M.L. Roukes, "Towards single-molecule nanomechanical mass spectrometry", *Nature Nanotechnology*, **4**, 445 (2009).
9. S.S. Verbridge, D.F. Shapiro, H.G. Craighead, J.M. Parpia, "Macroscopic Tuning of Nanomechanics: Substrate Bending for Reversible Control of Frequency and Quality Factor of Nanostring Resonators", *Nano Lett.*, **7**, 1728 (2007).
10. S.S. Verbridge, H.G. Craighead, J.M. Parpia, "A megahertz nanomechanical resonator with room temperature quality factor over a million", *Appl. Phys. Lett.*, **92**, 013112 (2008).
11. W.K. Hiebert, D. Vick, V. Sauer, M.R. Freeman, "Optical interferometric displacement calibration and thermomechanical noise detection in bulk focused ion beam-fabricated nanoelectromechanical systems", *J. Micromech. Microeng.*, **20**, 115038 (2010).
12. I. Wilson-Rae, R.A. Barton, S.S. Verbridge, D.R. Southworth, B. Ilic, H.G. Craighead, J.M. Parpia, "High-Q Nanomechanics via Destructive Interference of Elastic Waves", *Phys. Rev. Lett.*, **106**, 047205 (2011).
13. Q.P. Unterreithmeier, T. Faust, and J.P. Kotthaus, "Damping of Nanomechanical Resonators", *Phys. Rev. Lett.*, **105**, 027205 (2010).
14. T.P.M. Alegre, A.H. Safavi-Naeini, M. Winger, O. Painter, "Quasi-two-dimensional optomechanical crystals with a complete phononic bandgap", *Opt. Express*, **19**, 5658 (2011).